Journal of Volcanology and Geothermal Research 290 (2015) 63–74

Contents lists available at ScienceDirect

Journal of Volcanology and Geothermal Research

journal homepage: www.elsevier.com/locate/jvolgeores

Stable and unstable phases of elevated seismic activity at the persistently restless Telica Volcano, Nicaragua

Mel Rodgers [a,b,*], Diana C. Roman [c], Halldor Geirsson [d], Peter LaFemina [d], Stephen R. McNutt [b], Angelica Muñoz [e], Virginia Tenorio [e]

[a] University of Oxford, UK
[b] University of South Florida, USA
[c] Carnegie Institution of Washington, USA
[d] The Pennsylvania State University, USA
[e] Instituto Nicaraguense de Estudios Territoriales (INETER), Nicaragua

ARTICLE INFO

Article history:
Received 13 August 2014
Accepted 27 November 2014
Available online 4 December 2014

Keywords:
Telica
Low-frequency seismicity
Phreatic eruption
Open-system degassing
Closed-system degassing

ABSTRACT

Telica Volcano, Nicaragua, is a persistently restless volcano with daily seismicity rates that can vary by orders of magnitude without apparent connection to eruptive activity. Low-frequency (LF) events are dominant and peaks in seismicity rate show little correlation with eruptive episodes, presenting a challenge for seismic monitoring and eruption forecasting. A short period seismic station (TELN) has been operated on Telica's summit since 1993, and in 2010 the installation of a six-station broadband seismic and eleven-station continuous GPS network (the TESAND network) was completed to document in detail the seismic characteristics of a persistently restless volcano. Between our study period of November 2009 and May 2013, over 400,000 events were detected at the TESAND summit station (TBTN), with daily event rates ranging from 5 to 1400. We present spectral analyses and classifications of ~200,000 events recorded by the TESAND network between April 2010 and March 2013, and earthquake locations for a sub-set of events between July 2010 and February 2012. In 2011 Telica erupted in a series of phreatic vulcanian explosions. Six months before the 2011 eruption, we observe a sudden decrease in LF events concurrent with a swarm of high-frequency (HF) events, followed by a decline in overall event rates, which reached a minimum at the eruption onset. We observe repeated periods of high and low seismicity rates and suggest these changes in seismicity represent repeated transitions between open-system and closed-system degassing. We suggest that these short- and long-term transitions between open to closed-system degassing form part of a long-term pattern of stable vs. unstable phases at Telica. Stable phases are characterised by steady high-rate seismicity and represent stable open-system degassing, whereas unstable phases are characterised by highly variable seismicity rates and represent repeated transitions from open to closed-system degassing, where the system is unable to sustain steady open-system degassing. These observations have implications for seismic monitoring at persistently restless volcanoes as the recognition of unstable seismic phases may indicate the open-system degassing process cannot be sustained and explosions are likely.

1. Introduction

Persistently restless volcanoes (PRVs) (Stix, 2007) are characterised by highly variable rates of seismicity, persistent degassing and frequent explosions. PRVs do not experience clear 'background' or 'unrest' states, and instead experience phases of eruptive and non-eruptive behaviour that show little obvious correlation with geophysical measurements. For example, the 1999 sub-Plinian eruption of the persistently restless Shishaldin Volcano, Alaska was preceded by a short-lived seismic swarm, but much larger swarms occurred in other years with no subsequent eruptive activity (Petersen et al., 2006). Recognition of precursory seismic swarms is an important aspect of volcano monitoring, but the highly variable rates of seismicity observed at PRVs make forecasting eruptive activity based on changes in seismicity rates alone challenging, highlighting the need for an improved understanding of the processes and patterns of seismicity occurring at PRVs. In this study we aim to characterise seismicity at the persistently restless Telica Volcano, Nicaragua, during periods of eruptive and non-eruptive activity, and to investigate the volcanic processes that drive the transition between these two types of activity.

Telica Volcano exhibits unusual seismic activity before, during and after eruptions. Seismicity preceding the 1999 eruption of Telica declined in the months before the eruptive episode and also before large

* Corresponding author at: University of Oxford, UK. Tel.: +44 1865 272000; fax: +44 1865 272072.
E-mail address: mel.rodgers@earth.ox.ac.uk (M. Rodgers).

http://dx.doi.org/10.1016/j.jvolgeores.2014.11.012

explosions during the eruption (Rodgers et al., 2013). In 2009-2010 researchers from the University of South Florida and The Pennsylvania State University installed a network of seismic and continuous GPS (cGPS) stations on Telica (Fig. 1) to study its seismic and magmatic processes. In this study we analyse the seismicity at Telica over a three-year period from 2010 until 2013, including a period of phreatic eruptive activity in 2011. We document and interpret changes in event rates and event properties, including spectral content, over the three years of the network deployment, including changes in seismicity surrounding the 2011 eruption. In this study we find that rates of seismicity at Telica are highly variable, but that the pattern of seismicity surrounding the 2011 eruption shares certain similarities with the 1999 eruption, in that we observe a decline in seismicity in the months before the eruption. We propose a model for the long-term patterns of seismicity where the system transitions from stable to unstable phases, where stable phases represent periods of well-established open-system degassing and unstable phases represent periods of repeated transition from open to closed-system degassing.

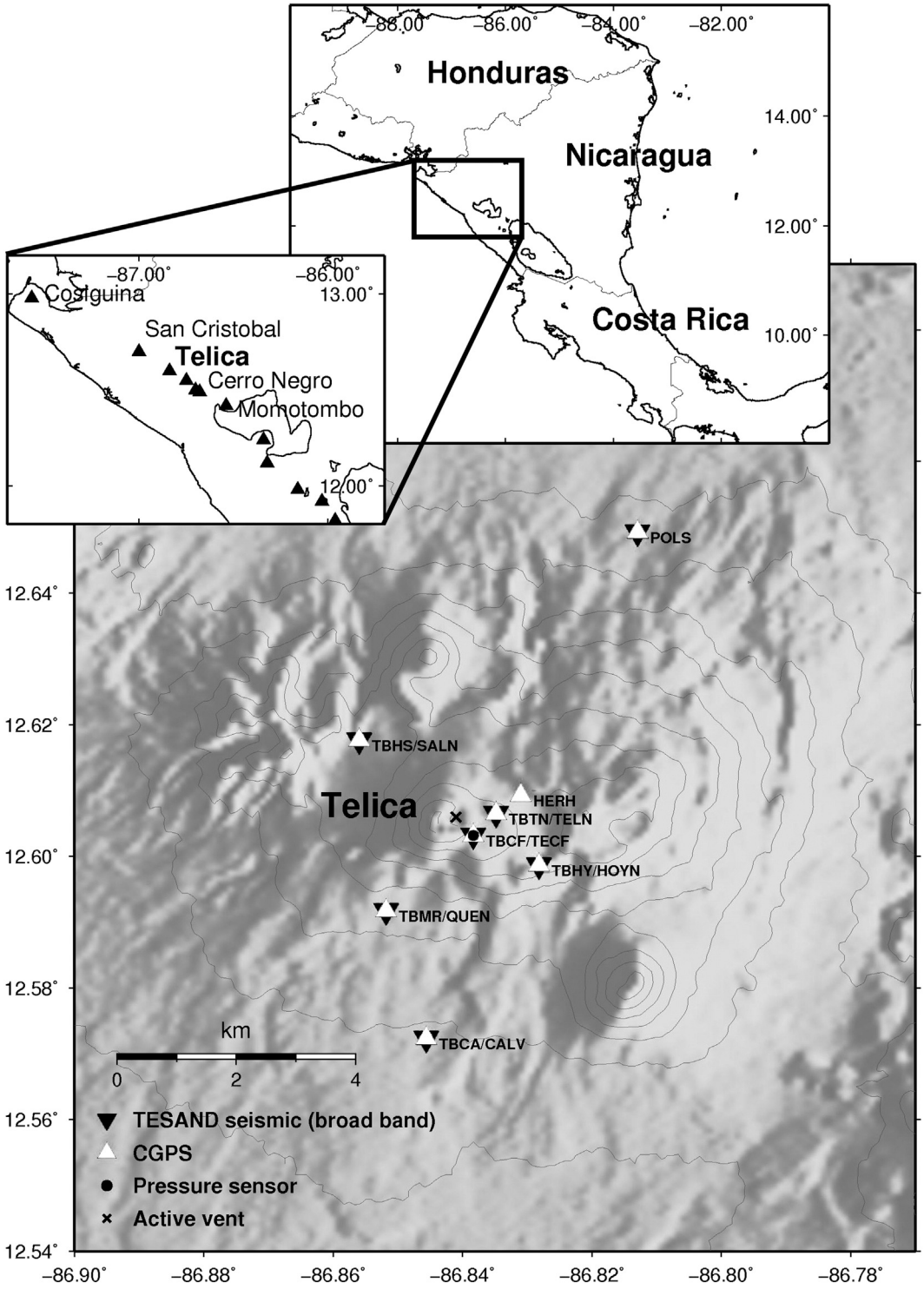

Fig. 1. Location of Telica Volcano and TESAND network stations: seismic stations (black inverted triangles), CGPS stations (white triangles) and pressure sensor (black circle). Inset map: Central America (right) and major volcanic centres of NW Nicaragua (left).

2. Background

2.1. Telica Volcano, Nicaragua

Telica is a basaltic-andesitic volcano in the Maribios range of the Central American volcanic arc (Fig. 1) where the Cocos plate subducts beneath the Caribbean plate. The Telica volcanic complex is an east-west trending series of volcanic craters, with the oldest (La Joya) pit crater at the eastern end and the currently active crater at the western end (Roche et al., 2001). Eruptive activity at Telica Volcano is characterised by small low-explosivity phreatic to phreatomagmatic vulcanian eruptions (VEI 1-2) every few years, however large eruptions have occurred at Telica (Siebert and Simkin, 2002). The largest historical eruption occurred in 1529 (VEI 4) and produced the only historically-recorded lava flow. Telica's geology, showing multiple lava flows, thick scoria layers and pyroclastic deposits suggests earlier periods of intense eruptive activity. In 1993 the first permanent seismometer (TELN) was installed 0.4 km from the active vent of Telica, and since then highly variable rates of seismicity have been observed. On average ~4000 events per month were recorded between 1997 and 2009 by this summit station (Fig. 2). The rate varies from less than ten events for the entire month of June 1998, to almost 20,000 events for the month of May 2004 (Tenorio, 1993), but peaks in seismicity are generally not associated with episodes of eruptive activity.

2.2. Eruptive activity

Eruptive activity during the study period was dominated by a three-month-long series of phreatic vulcanian explosions in 2011. A minor period of ash emission occurred on the 13th and 14th January 2013 when small, diffuse ash plumes were observed, but these plumes barely rose above the crater rim. The 2011 eruption episode started on the 7th March 2011 when the first ash emissions were observed, and small explosions were reported in March and April 2011 (Geirsson et al., 2014). Three distinct explosions on the 8th May 2011 are considered to reflect the start of a more energetic explosive period. Some of the most energetic explosions of the 2011 eruptive episode were observed on the 18th May and on the 21st May 2011, and produced eruption plumes up to 2 km elevation and sustained ash emissions for up to 30 minutes. Eruptive activity then waned after the 24th May 2011 and the eruption ended by mid-June 2011. An average SO_2 flow rate of 115 ($\pm$ 100) tons/day was measured between January and March 2010; an average of 140 ($\pm$ 110) tons/day was measured during the eruptive episode (May-June 2011) and a single DOAS (Differential Optical Absorption Spectroscopy) measurement of 66 tons/day was recorded on the 16th March 2011 (Geirsson et al., 2014). Crater floor temperature measurements indicated a stable temperature of 200-300 °C in early 2010, which dropped to ~130 °C in February-March 2011 and then increased to 590 °C in June 2011 (Geirsson et al., 2014). Ash analysis (Major element concentrations; X-ray diffraction) suggests that the erupted material was altered prior to eruption and the existence of accretionary lapilli in the deposits suggests a phreatic eruption (Geirsson et al., 2014). The TESAND cGPS recorded only tectonic deformation between early-2010 and mid-2012 and the lack of any deformation signal attributed to volcanic processes at Telica suggests that any intrusion of magma that may have occurred was either too small or too deep to be observed geodetically, or that any build-up of pressure as a result of sealing was also too small to be observed (Geirsson et al., 2014).

3. Seismic data analysis

3.1. The TESAND experiment

In 2009-2010 the TElica Seismic ANd Deformation (TESAND) network was installed at Telica Volcano, Nicaragua. This network consists of six intermediate-band (30 second) seismometers (Guralp 6TD/6 T), one pressure sensor (Chaparral 25 V) and ten cGPS (Net RS) stations (Fig. 1). The first seismometer was installed in November 2009 at station TBTN (Figs. 1 and 3), the remaining five seismic stations and the majority of the cGPS stations were installed in March 2010, and the pressure sensor (TBCF) was installed in June 2010 (Fig. 3).

The seismic network design was determined by the location of pre-existing concrete instrumentation bunkers, which provide critical security for the instruments and peripherals. Two of the TESAND stations (TBTN and TBCA) were co-located with existing INETER short-period seismic stations (TELN and TEL3). The closest station, TBCF, is 0.2 km from the active vent and houses a seismic and pressure sensor. The location of the seismic stations gives good coverage for local events, with a maximum azimuthal gap of 130° around the vent and distances from the vent of between 0.2 km and 3.5 km (discounting station TBPV, which was only operated for the first four months of this study).

The continuous seismic data analysed in this study were recorded with a sampling rate of 100 Hz at station TBCF (the co-located seismic and infrasound station), and 50 Hz at all other seismic stations. Seismic data were stored locally on the instruments and downloaded every three months during maintenance visits. TBTN was chosen as the primary station for single-station analyses due to its relative proximity to the vent, minimal data gaps (Fig. 3) and long-term continuity with the short-period INETER station TELN.

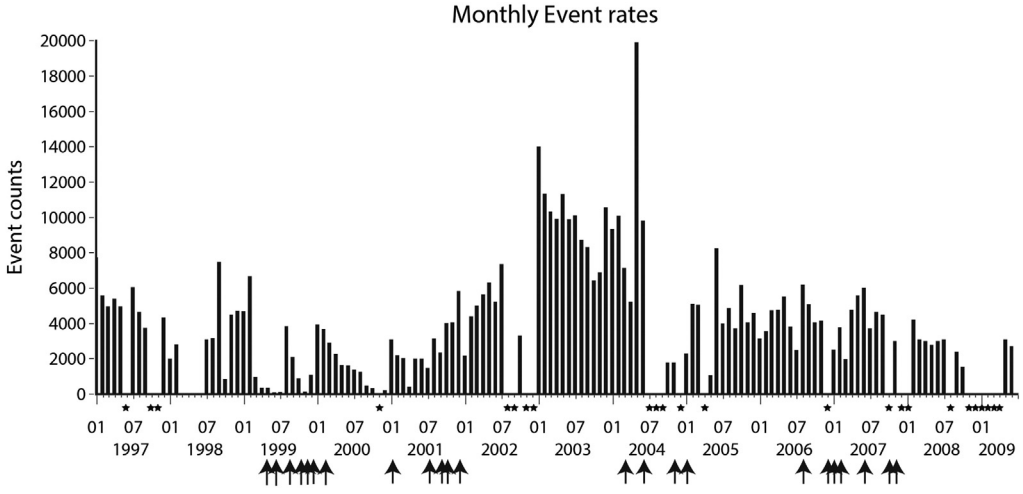

Fig. 2. Monthly event rates from 1997 to 2009, reproduced from INETER monthly bulletins. For details on event detection parameters see Tenorio, (1993). Months for which there are no published data are indicated by asterisks under the time-axis. Months during which explosions/ash emissions were reported are indicated by arrows.

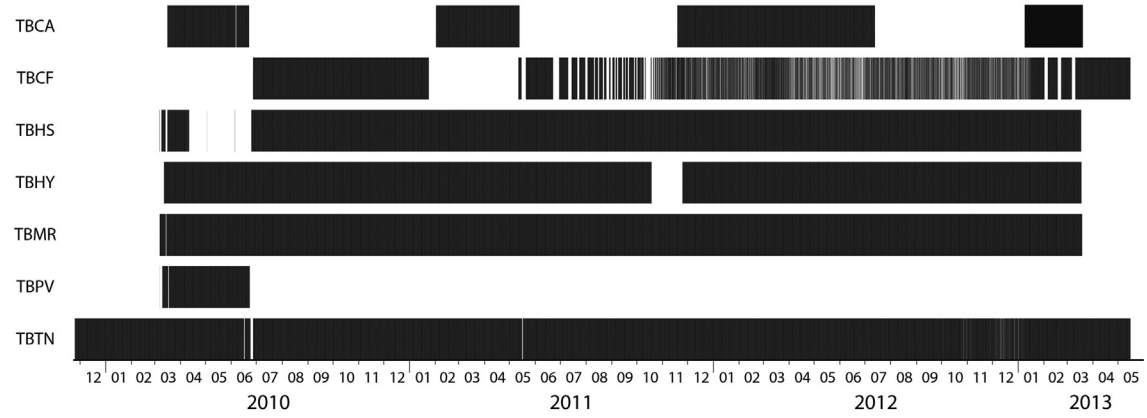

Fig. 3. Station operation time periods for all the TESAND network seismic stations are indicated by black horizontal bars. Data gaps of less than one hour are not displayed. Note that power problems occurred at station TBCF from 2011 to March 2013.

3.2. Event detection

We used Antelope Environmental Data Collection Software (http://www.brtt.com) to create a catalogue of event detections and associated waveforms from continuous seismic data from our entire network. The Antelope event detection method uses a multiple station, short-term average/long-term average (STA/LTA) (Table 1) approach to detect candidate seismic events. STA/LTA detections were run twice over the data at two different filter bands: A low-frequency filter, and a high-frequency filter (See Table 1). When detections occur on more than a given number of stations at the same time (we used a three station minimum and a 1.5 second time window for associated detections on multiple stations) a grid search is performed to attempt to define an origin point for the earthquake, and the event is added to the catalogue only if an origin point can be found within the specified grid. This multi-station STA/LTA approach minimises the chance of noise on a single station being catalogued as an event, and the grid search approach minimises regional earthquake inclusion in the catalogue, and also minimises the chance of simultaneous noise from multiple stations being catalogued as an event. Due to the necessary prerequisite that the event must be detected at multiple stations, this detection method will miss small events that would only be detected at the closest stations (e.g., station TBTN). As with any detection method, event rates will be affected by station outages.

As small events that are only visible at the closest stations may be missing from the Antelope catalogue, we also compiled a single-station detection catalogue from station TBTN, which is 0.4 km from the active vent (Fig. 1), and which has a slightly longer continuous record of data than the other TESAND stations. The vertical component of the continuous seismic data was high-pass filtered at 0.5 Hz to remove microseismic noise, and an STA/LTA event detection algorithm (AECAP, Powell, 2004) was used to detect events (Table 1).

Table 1
STA/LTA event detection parameters. STA Window: Time window for the short-term average time. LTA Window: Time window for the long-term average. Threshold on: Ratio of STA/LTA at which an event is triggered. Threshold off: Ratio of STA/LTA at which event is de-triggered. Filter: Frequency range at which data is filtered before event detection. AECAP column shows parameters used for the single station detection only. ANTELOPE (HF) and (LF) columns show parameters used for the Antelope multi-station detection method where detections were made for the same data using two different filter bands.

Parameter	AECAP	ANTELOPE (HF)	ANTELOPE (LF)
STA window (seconds)	1	1.4	2.3
LTA window (seconds)	60	7	11.5
Threshold on	8	3.4	2.4
Threshold off	3	1.7	1.7
Filter (Hz)	0.5–20	3–18	0.5–10

3.3. Spectral analysis and amplitude

3.3.1. Dominant frequency and amplitude

The dominant frequency of every event in the Antelope catalogue was calculated based on the Fast Fourier Transform (FFT) of a 12 second window around the largest-amplitude peak in the waveform (4 seconds before, 8 seconds after). The largest peak in the power spectral density between 1 and 15 Hz was chosen as the dominant frequency for the event (Fig. 4). The amplitude of each event was calculated by taking half the maximum peak-to-peak amplitude of each waveform (Fig. 4a).

3.3.2. Ratios of high-to-low spectral energy

Average spectral amplitudes for high and low frequency bands were used to determine the ratio of high-to-low spectral energy 'band-ratios' for every event in the Antelope catalogue (Fig. 4b) (Buurman and West, 2010; Thelen et al., 2010). The dominant frequencies at five of the six stations demonstrate similarity between stations with many events having dominant frequencies below 6 Hz. The 6th station shows an anomalous absence of any low-frequency energy and hence is not considered for this analysis (See Section 3.4). Based on this similarity across stations, frequency bands of 1–6 Hz (low) and 6–11 Hz (high) were chosen to determine band-ratios. As many events had dominant spectral energy around 4 to 5 Hz, choosing the more conventional 5 Hz threshold (Lahr et al., 1994) would have caused events with energy at ~5 Hz to be too close to the threshold, potentially allowing small variations in the frequency of the events to have a significant effect on the ratio. For every event the base-2 log of the ratio of the high-frequency spectral amplitude band to the low-frequency spectral amplitude band was calculated (Buurman and West, 2010; Thelen et al., 2010). This method was chosen to give events with dominantly low-frequency energy a negative value, events with dominantly high-frequency energy a positive value, and events with equal amounts of low and high energy a value of zero. By choosing log base 2, the negative and positive ratios then give an equal indication of the relative amounts of high to low energy, with a value of 1 indicating there is twice as much high-frequency energy as low-frequency energy, and a value of -1 indicating there is twice as much low-frequency energy as high-frequency energy.

3.4. Classification

Consistent event classification is an important part of identifying changes in seismicity, and of relating seismicity characteristics to source processes (Minakami, 1974; Lahr et al., 1994; McNutt, 1996). In volcano observatories, event types are often determined manually by a seismic analyst. While there are advantages to this approach in that every event is assessed by an analyst such that noise is unlikely to be

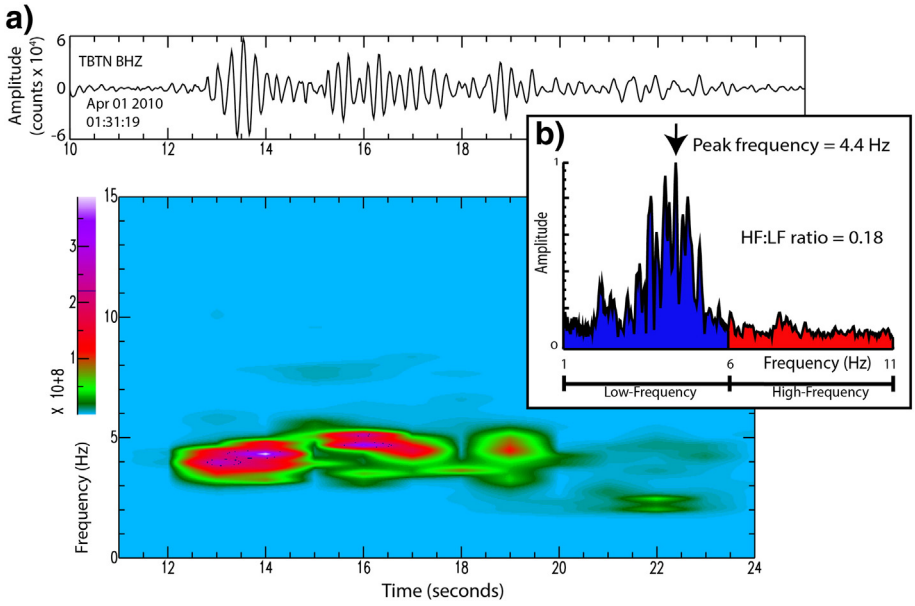

Fig. 4. a) Waveform (top), spectrogram (bottom), and **b**) periodogram (inset) of example low-frequency event from the 1st April 2010 from station TBTN. The spectrogram was produced using a window size of 2 s, overlap of 1 s and FFT size of 256 samples.

catalogued as an event, there can be inconsistencies in event classification between different analysts. Also, at volcanoes such as Telica that have hundreds of events per day, it is impractical to analyse this amount of data manually. Automated classification of events provides consistency across long periods of data and provides a systematic and automated approach for efficiently analysing many thousands of events.

In this study classifications were assigned to detected seismic events based on their band-ratios: If an event had more low-frequency energy than high-frequency energy it was classified as a low-frequency event (i.e. HF:LF ratio <1) (Fig. 5a). If an event had more high-frequency energy than low-frequency energy it was classified as a high-frequency event (i.e. HF:LF ratio >1). The small number of events (~30 events out of a total of >200,000 events) where the HF:LF ratio was equal to 1 were included in the LF classification.

Classification across the network occurred through a two-stage process. Rather than determining the average band-ratio across the network, which could potentially be skewed if there was noise on one or more stations, we employed a system in which events were classified at each station and then those classifications were compared across three stations. Stations TBTN, TBMR and TBHY were chosen for the classification process as these have the most complete continuous waveform data (Fig. 3). Station TBHS was considered as a potential station for this process, but was discarded due to an anomalous absence of low-frequencies in the dominant-frequency plot, perhaps indicating a site effect at this station or a path effect in the azimuth to this station (McNutt, 2005, and references therein). Stations TBCF and TBCA were not used due to large data gaps. To minimise noise or path effects influencing the classification, for an event to be given a final class it had to have the same classification at two or more stations. We chose to use two stations for this classification, rather than all three stations, so that any events that were noisy at one station were not unnecessarily removed from the catalogue.

3.5. Earthquake locations

To make an initial assessment as to whether or not the location of seismic events varied surrounding the 2011 eruption we located a sub-set of earthquakes from the Antelope catalogue for the period 1st July 2010 to the 29th February 2012. Of the 200,000 earthquakes in the catalogue we selected the 100 largest-amplitude earthquakes per month (based on amplitude at TBTN) in this 20-month period (See Section 4.4 for discussion of this selection method). Because events in the catalogue are typically small and emergent, selection of the 100 largest amplitude events per month gave us the best chance of obtaining well-constrained locations.

For events in our sub-sampled catalogue we manually picked P-wave arrivals, and where possible S-wave arrivals, using two iterations of picks – i.e. all events in the catalogue were initially picked, the

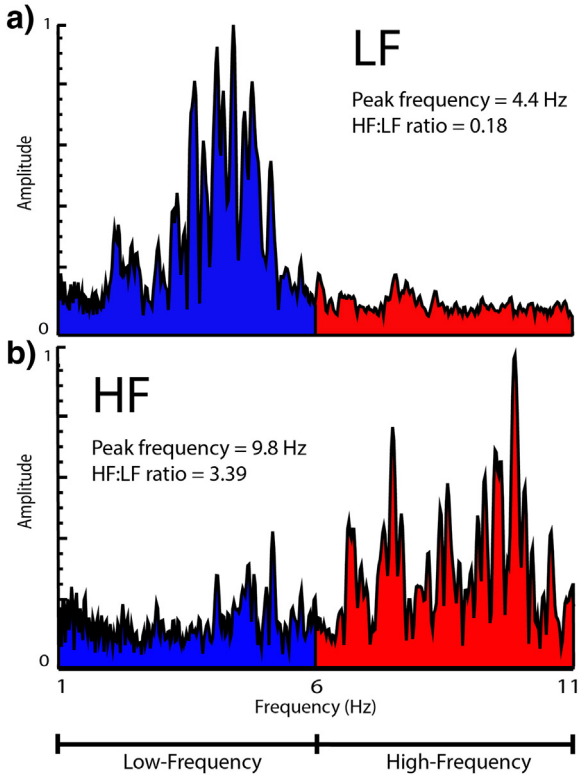

Fig. 5. Normalised periodograms of two selected events from station TBTN. Frequency amplitudes are indicated by colours: Blue indicates energy below 6 Hz; red indicates energy above 6 Hz. a) Low-frequency event from 1st April 2010 at 01:31. Peak frequency = 4.4 Hz, HF:FL ratio = 0.18, b) High-frequency event from 4th September 2012 at 20:36. Peak frequency = 9.8 Hz, HF:LF ratio = 3.39.

catalogue was then reviewed and where necessary re-picked after completion of the first iteration. Events were located using the program HYPOCENTER (Lienert and Havskov, 1995). We used the same 1D velocity model as used by the Alaska Volcano Observatory for Shishaldin, Alaska (McNutt and Jacob, 1986; Dixon et al., 2006) as Shishaldin shares many similarities to Telica in terms of composition (they are both basaltic-andesite volcanoes) and eruptive style (they both have frequent small eruptions).

4. Results

4.1. Single-station total event counts

To demonstrate the large variation in seismicity rates over the study period we plot total daily seismic event rates vs. time for station TBTN (Fig. 6). In total over 416,000 events were detected by our single-station STA/LTA method at this station. Over the entire study period from the 26th November 2009 to the 15th May 2013 there is an average seismicity rate of 329 events per day. Swarms were identified by calculating a 10-day moving average (Fig. 6) and any peaks over a threshold of twice the average seismicity rate (i.e. 658 events per day) were defined as a swarm. The daily event rate shows considerable variation, ranging from a minimum of 5 events on the 17th March 2011, to 1419 events on the 21st March 2013.

At the beginning of the study period the event rate is fairly constant, with an average of 533 events per day between November 2009 and the end of August 2010. There is a short-lived peak in event rates in August 2010, with a high of 994 events on the 25th August 2010. From October 2010 event rates start to decline, reaching a minimum of 5 events on the 17th March 2011, ten days after the start of the 2011 eruptive episode. Visual inspection of waveforms and a lack of any elevated RSAM (Endo and Murray, 1991) during this drop in seismicity indicate that this event rate drop is real and cannot be attributed to tremor or other non-detected signals saturating the STA/LTA detection algorithm. All operational stations were functioning correctly and as such we can also rule out any network bias as a cause of the event rate drop.

Approximately two weeks after the onset of the eruption in March 2011, the event rate starts to increase again. An increase occurs during the onset of the more energetic phase of the eruption on the 8th May 2011. The event rate reaches a high in June 2011, shortly before the end of the eruptive episode, and then decreases throughout July and August 2011. After reaching a post-eruption minimum at the beginning of September 2011 we observe two prominent swarms lasting approximately one to two months each. These swarms occur in October/November 2011 and February 2012 and reach maxima of 1200 and 1400 events per day. After the second swarm, event rates start to decline for the next eight months, from ~250 events per day in April 2012 to ~10 events per day in December 2012. On the 13th and 14th January 2013 a minor period of ash emission was observed, after which event rates start to increase again, and after a brief drop in event rates in February 2013, a swarm of events occurs from March - May 2013. The maximum event rate of the entire study period is observed during this swarm, reaching 1419 events on the 21st March 2013. The event rate decreases after the peak in March 2013 and continues to decrease until the end of the study period on the 15th May 2013. We searched for but did not find any annual or seasonal component to the seismicity rates nor found any correlation with the limited rainfall data available.

4.2. Spectral analysis and amplitude

To demonstrate the variation in spectral content and event amplitude over time we plot dominant frequency, band-ratio and amplitude for every event in our event detected catalogue from stations TBTN and TBMR (Figs. 7 and 8). Data for these analyses are from the Antelope catalogue, which runs from the 1st April 2010 until the 18th March 2013, and contains almost 218,000 events. Station TBMR is on the opposite side of the vent from TBTN, such that any path effects predominantly affecting only one side of the volcano would hopefully be evident in our analysis, however we note that we cannot account for path effects over the entire edifice (Fig. 1).

Stations TBTN and TBMR show similar temporal variations in spectral content and amplitudes during the study period. Between April and August 2010, low frequency energy dominates the catalogue. The dominant frequency plots (Figs. 7a and 8a) indicate that most events have frequencies below 6 Hz (91% for TBTN) and the band-ratio plots (Figs. 7b and 8b) show that events have ratios mainly below -1 (i.e., events with more than twice the amount of low-frequency energy to high-frequency energy) (84% for TBTN).

At the beginning of September 2010 there is a marked change in spectral content. There is an increase in the number of events with frequencies of 6–15 Hz (Figs. 7a and 8a) and the band-ratios during this period show a range of ratios from −4 to 2 (Figs. 7b and 8b), suggesting events are occurring across a broad range of frequencies. Co-incident with this pulse of events with a broad range of frequencies, the amplitudes of the events decrease (Figs. 7c and 8c). This broadband pulse is followed by a cessation of events with frequencies in the 1–3 Hz range at TBTN and in the 1–2 Hz range at TBMR and can be seen in the band-ratios as a jump in the lower limits from ~−3 to ~−2. In the six-month period before the onset of the eruption, from October 2010 to March

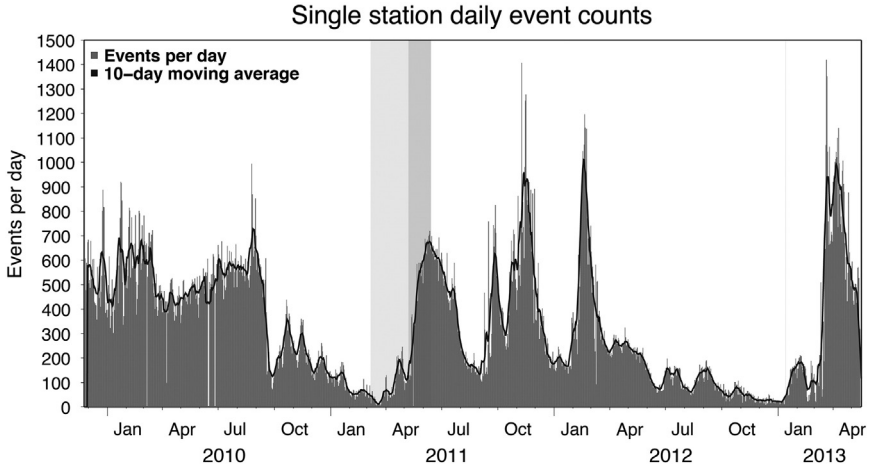

Fig. 6. Total daily single-station seismic event counts from November 2009 until May 2013 from station TBTN (dark grey vertical bars) with a corresponding 10-day moving average event-rate (black line). The 2011 eruption period is marked by grey shaded boxes, the more energetic phase of the eruption in darker grey, and the January 2013 ash emission is marked by a light grey vertical line.

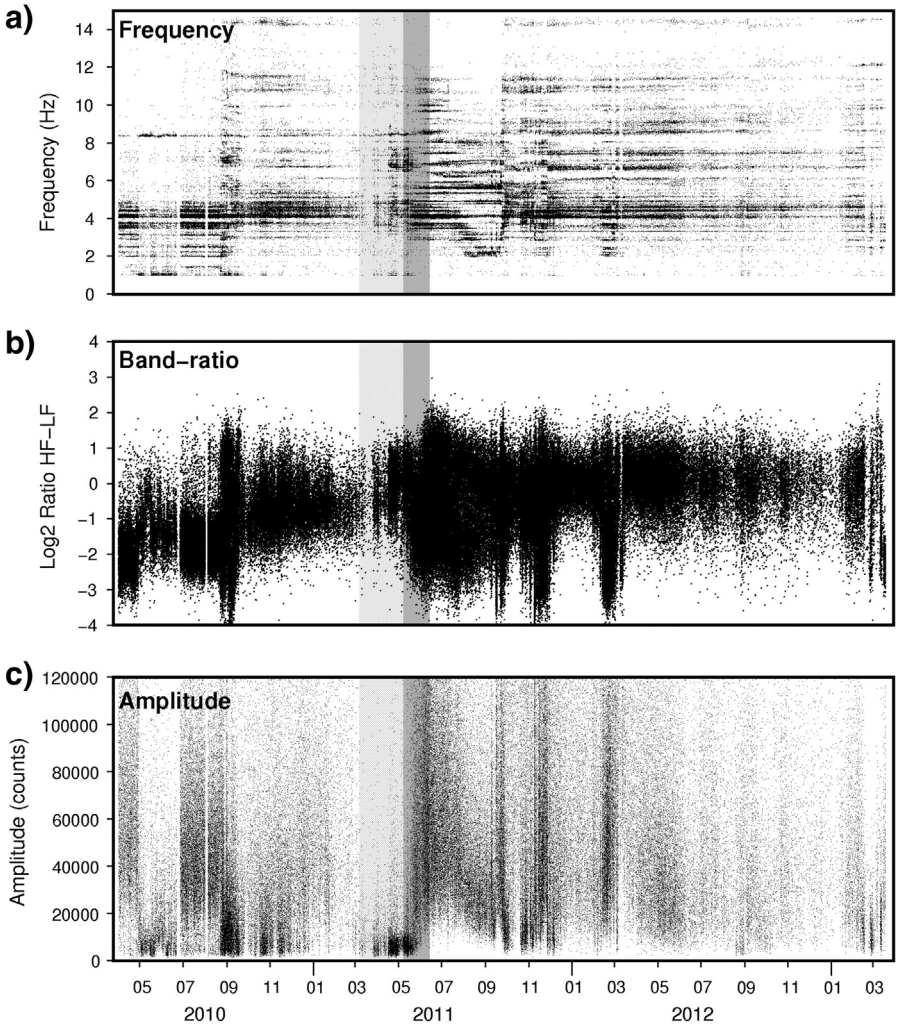

Fig. 7. Multi-parameter information for each event at station TBTN from April 2010 until March 2013. a) Dominant frequency, b) frequency band-ratio, c) amplitude. The eruption period is marked by grey shaded boxes, the more energetic phase of the eruption in dark grey.

2011, there is a narrowing in the range of band-ratios and events with dominant frequencies of 6—15 Hz disappear. The amplitude of events between October 2010 and March 2011 show a considerable amount of scatter, but there is an overall increase in the amplitude of the events until the end of January 2011, before a reduction in amplitude in February.

At the onset of the energetic phase of the eruption, the band-ratios indicate an increase in the low-frequency content of the events and the amplitudes increase (Figs. 7 and 8). Towards the end of the eruptive episode, high-frequency content is observed as a peak in the band-ratios; this is also observed as a reappearance of events with dominant frequency in the 6–15 Hz range.

The two swarms in November 2011 and February 2012 that are seen as large increases in event rates (Fig. 6) can also be seen in the amplitude and the band-ratio plots (Figs. 7b, c and 8b, c). Amplitudes increase during these swarms and band-ratios show broadband pulses of events with ratios between −4 and 1.5. These swarms are not seen clearly in the dominant frequency data (Figs. 7a and 8a); they appear only as perturbations to the dominant bands of frequencies. After the swarms, from April 2012 onwards, there is a narrowing of the band-ratios into the HF range, and a decrease in amplitudes (Figs. 7 and 8).

4.3. Event rates of classified events

Daily event rates classified by frequency content reveal interesting changes in the pattern of seismicity at Telica (Fig. 9) that are not readily evident from analysis of total seismicity (Fig. 6). LF events dominate the catalogue, with an average of 144 events per day, compared to 54 HF events per day (Fig. 9). In April 2010, at the start of the catalogue, LF event rates are ~200 events per day and there are almost no HF events. The drop in LF event rates between mid-April and June 2010 corresponds to a period when station TBHS was not operational (Fig. 3) and TBCF had not yet been installed, leaving only three proximal stations in the network (TBTN, TBMR and TBHY). Because the Antelope detection parameters require an event to be detected on at least three stations, we believe this drop in April 2010 and subsequent increase in June 2010 of the LF event rate to be a consequence of the network configuration.

This supposition is further supported by the consistency of event rate from the single-station detections at TBTN during this time (Fig. 6).

In late August 2010 there is a spike in LF events (Fig. 9), with 750 events on the 25th August 2010, followed seven days later by a smaller peak in HF events. Between October 2010 and March 2011 there is an overall decline in event rates for both LF and HF events. The eruptive episode starts on the 7th March 2011 and the event rate minimum occurs nine days later, with three LF and zero HF events. The LF event rates start to increase after this minimum and reach a peak on the 11th June 2011, whereas the HF rates peak almost a month earlier, at the onset of the energetic phase of the eruption.

The swarms in October/November 2011 and February 2012 are clearly seen in the LF event rate. The maximum LF rate of the study

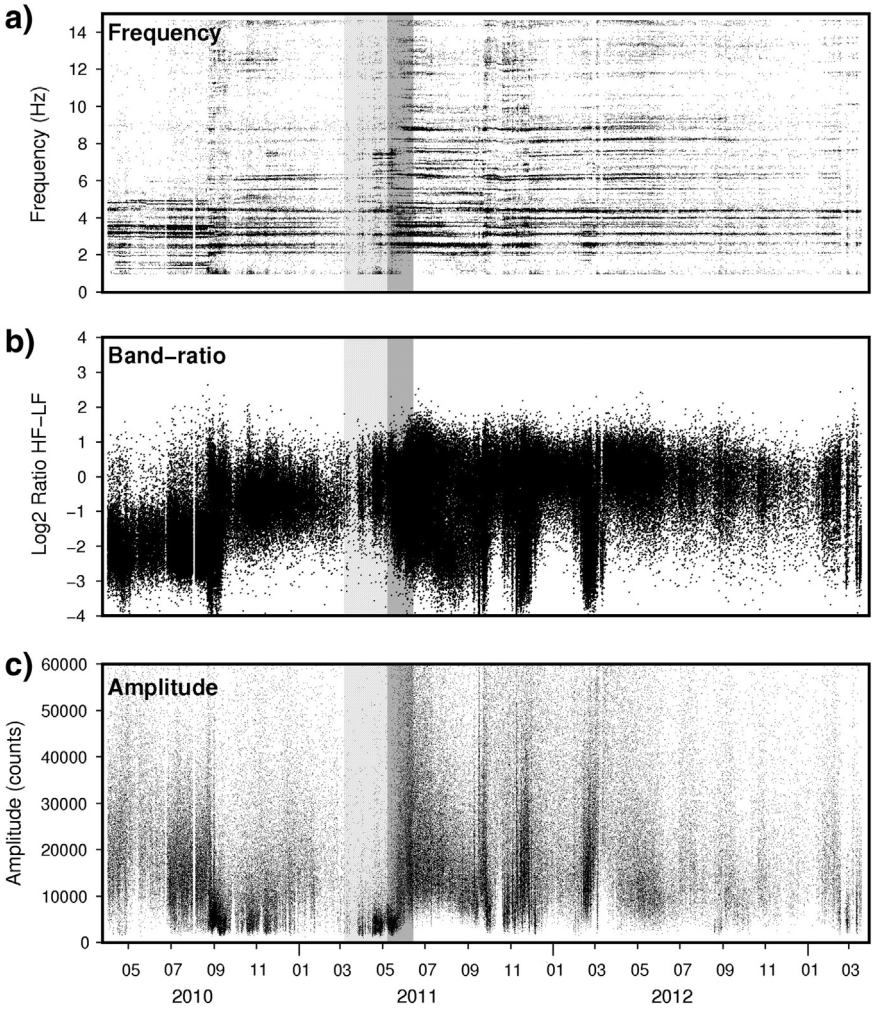

Fig. 8. Multi-parameter information for each event at station TBMR from April 2010 until March 2013. a) Dominant frequency, b) frequency band-ratio, c) amplitude. The eruption period is marked by grey shaded boxes, the more energetic phase of the eruption in dark grey.

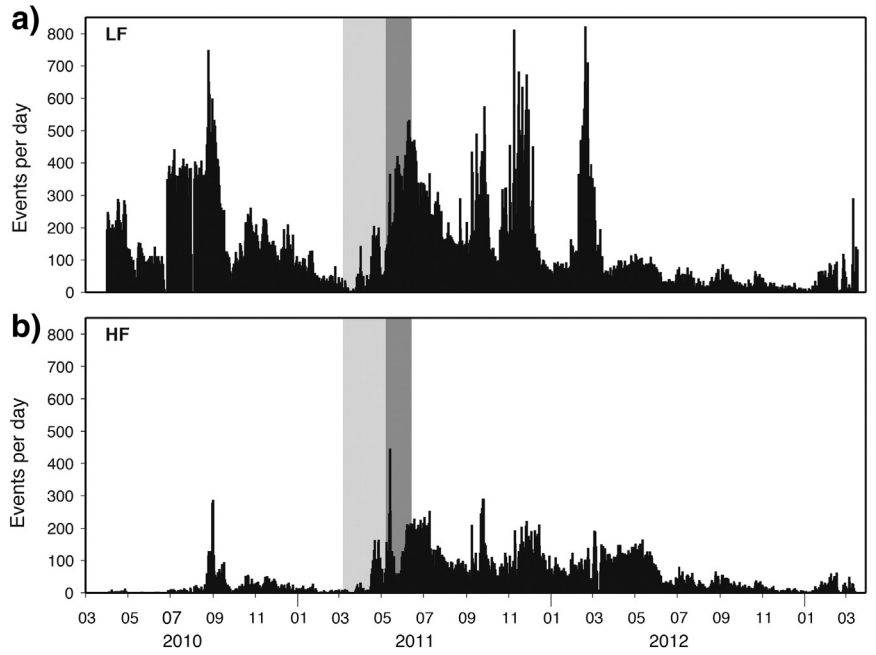

Fig. 9. Daily event rates for the LF and HF classifications used in this study. a) LF events, b) HF events. The eruption period is marked by grey shaded boxes, the more energetic phase of the eruption in dark grey.

period occurs during the February 2012 swarm. The HF event rates remain high during these swarms and over the one-year period from June 2011 to June 2012 the daily average HF rate is 111 events per day. After May 2012 both LF and HF event rates start to decline, with an average of only 32 LF events per day and an average of 25 HF events per day between June 2012 and December 2012. A final swarm of events began towards the end of the study period (as seen from the single-station detections (Fig. 6)), but data from the full network were not available after the 18th March 2013.

4.4. Earthquake locations

Due to the emergent onsets of the earthquakes (e.g. Fig. 4), low amplitudes, shallow origins, and velocity model uncertainties, very few high-quality locations were obtained. Of the 2,000 events that were picked and located only 207 met our selection criteria of azimuthal gap <180°, RMS <0.2 s, horizontal and vertical uncertainties (as output by HYPOCENTER) <5 km, and number of stations >3 (S-wave picks were not required). Of these 207 events the average RMS was 0.06 s, the average horizontal error was 1.1 km, the average vertical error was 2.2 km, and there was no difference in error between HF and LF events.

Naturally, based on the azimuthal gap criteria, all located events are within the network and the event locations cluster beneath the vent, with the majority of the events located within a 500 m radius of the vent (Fig. 10). All events are shallow and no events occur below 2 km depth below datum, where the datum is taken as 1 km above sea level and is approximately the summit elevation of Telica. Classifications from Section 3.4 were used for these events, and events that had been discarded from that classification system were given the classification from station TBTN. There appears to be little horizontal difference in the locations of LF and HF events, but HF events appear to be slightly shallower than the LF events, although this could be attributed to attenuation of deeper HF events.

Selection of the 100 largest-amplitude events per month at station TBTN may have introduced a bias into the locations. We are choosing to only locate the largest events and thereby ignoring the locations of smaller events; however, given the small and emergent nature of the events it is unlikely we would have been able to locate any but the largest amplitude events. Another concern with the selection of the 100 largest events per month at station TBTN is that we are introducing a depth bias (i.e., the largest amplitude events might be just the shallowest events and deeper events of the same size are being ignored). There is also likely to be a location bias given the network configuration. We cannot reliably locate anything outside of our network, in

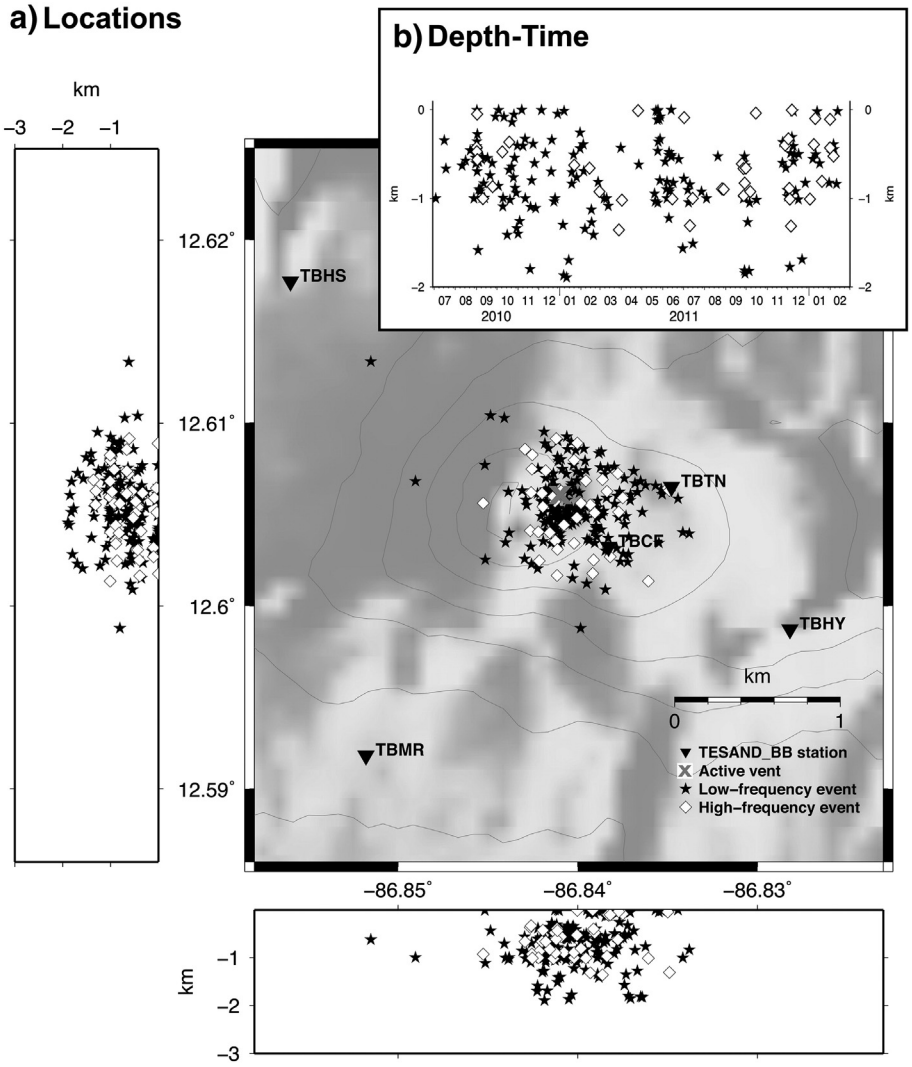

Fig. 10. Locations and depth cross-sections of the 207 well located events from the 1st July 2010 until the 29th February 2012. Depths shown are below a datum that is taken as the summit elevation of Telica (~ 1 km a.s.l.). TESAND seismic stations are shown by inverted black triangles, LF events shown by black stars, HF events by white diamonds. The active vent of Telica is shown by a grey cross. Inset (top right) shows depth-time plot of all events.

particular as we have no distal station to the northeast, we are limiting the boundaries of our locatable area to ~0.5 km northeast of the vent (this can be seen in the locations as the artificial straight line cut off of events between TBTN and TBHS (Fig. 10)).

5. Discussion

Our results support the general hypothesis of Geirsson et al. (2014), who suggest that temporary sealing of the hydrothermal system at Telica and subsequent failure of the seal drove the 2011 episode of phreatic vulcanian activity. In this study we re-analysed and re-classified seismic events using band-ratios and spectral information from multiple stations. Our results are consistent with observations presented by Geirsson et al. (2014), which were based on preliminary classifications of a subset of the TESAND seismic event catalogue, that a sharp decrease in the rate of LF seismicity, accompanied by the sudden onset of HF events, preceded the 2011 eruption by approximately six months (Fig. 9). LF seismicity may be attributed to resonance of a magmatic and/or hydrothermal fluid cavity (Chouet and Matoza, 2013). At open-vent volcanoes such as Telica, which exhibit high levels of degassing, unsteady or pulsatory transportation of either magmatic of hydrothermal fluids through a system of shallow conduits and/or cracks is a plausible source for LF seismicity (Rodgers et al., 2013). HF events at Telica may be similar to high-frequency 'volcano-tectonic' microseismic events observed at volcanoes worldwide (VTs). VTs can represent shear failure of rock in response to stress changes induced by changes in fluid pressures in a magmatic system (Roman and Cashman, 2006) and a similar pressurisation could occur in a sealed hydrothermal system. Telica is being actively sheared by tectonic stresses (Geirsson et al., 2014) and local faults within the edifice may be close to failure. Under such stress conditions an influx of new gas or new hydrothermal fluids could lower the effective normal stress on these local faults and promote shear failure (Byerlee, 1978). We find evidence in our newly reclassified event catalogue that is consistent with the hypothesis of Geirsson et al. (2014), in that sealing (indicated by a drop in LF events) and pressurisation (indicated by the onset of HF events) of the shallow hydrothermal system preceded and likely drove a series of phreatic explosions, and a return to high rates of LF seismicity after the eruption (Fig. 11). However, we note the gradual decline in HF seismicity in the six months preceding the eruption is inconsistent with a pressurising magmatic-hydrothermal system, which should lead to an increasing rate of HF seismicity before failure (Voight, 1988; Voight et al., 1999; Roman and Cashman, 2006; Kilburn, 2012). The implication that failure of a strongly sealed and pressurised magmatic-hydrothermal system was not the immediate cause of the 2011 eruptive episode is consistent with the low energy of the explosions and lack of deformation surrounding the eruption observed by Geirsson et al. (2014). One possible explanation for the lack of increasing HF seismicity is that the sealed and pressurising source was sufficiently shallow that deformation was localised to the crater floor (hence not detectable by our network) and that the weak or poorly-consolidated shallow material surrounding the pressurising source failed aseismically, resulting in a paucity of detectable HF events. Alternatively, a detailed analysis of the seismic and infrasound signatures of one of the strongest explosions by Geirsson et al. (2014) suggests that the explosion was not triggered by sudden brittle failure of a seal in an over-pressurised magmatic/hydrothermal gas system, but by a small pulse of gas that triggered sustained venting. The small gas pulse may have broken through a weak seal, and changes in circulation of high-temperature fluid may have also played a role. The first possibility implies that HF hypocentres should be observed to migrate upwards, while the second implies that a pulse of gas should be observed immediately prior to explosions. While our current set of observations are unable to differentiate between these two models, future work at Telica will provide the observations necessary to test both hypotheses.

The long-term persistence of variable seismicity rates during our nearly four-year-long study period suggests that instability in the shallow system continued after the 2011 eruption, and perhaps past the end of the study period. Following the end of the 2011 eruption we observe a series of strong LF swarms, the first of which commences during the end of the eruptive phase and has a peak rate comparable to the pre-August 2010 LF event rates. This first post-eruption LF swarm may reflect a temporary return of the magmatic-hydrothermal system to a state of open-system degassing (Fig. 11). However, in contrast to pre-August 2010 seismicity patterns, LF swarms from May 2011 onwards were accompanied by high HF rates, suggesting that some mechanism of sealing and/or pressurisation was still able to periodically close gas pathways. Following the LF swarm in February 2012, both LF and HF events began a nine-month long decline in seismicity rates that culminated in several small diffuse ash emissions in January 2013. Together

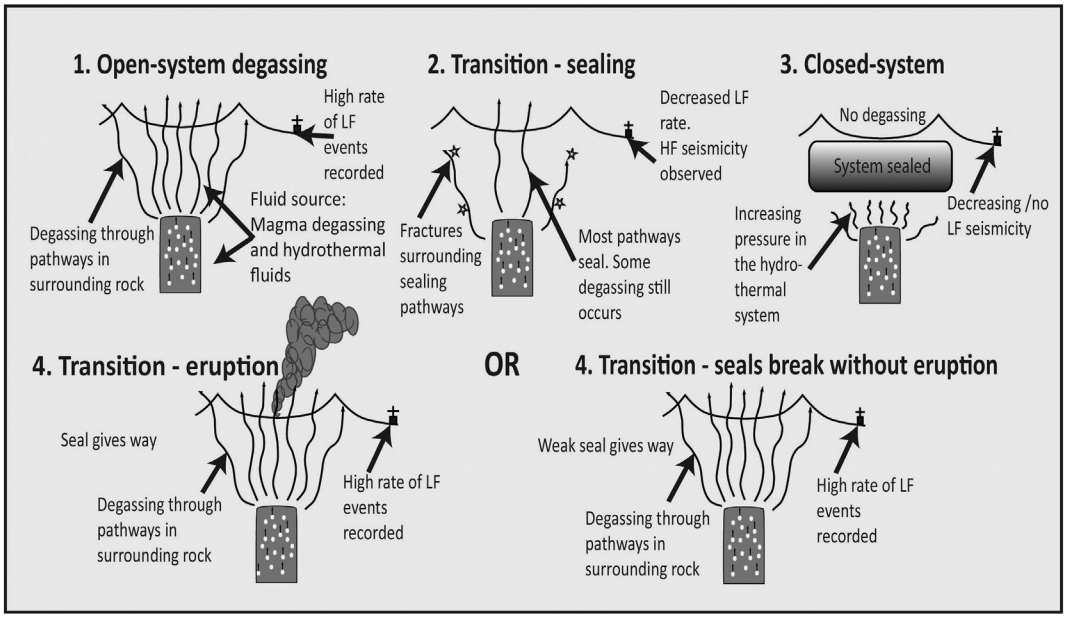

Fig. 11. Interpretation of the open-system to closed-system transition hypothesis with sealing of degassing pathways. Open-system degassing is followed by a transition period and gradual sealing of the degassing system. The closed-system can then transition back to open-system degassing either with or without eruption.

these observations suggest that the shallow magmatic-hydrothermal system at Telica continued to experience transitions between open and closed system degassing after the 2011 eruption period. It is possible that a longer period of observation at Telica will demonstrate an eventual return to stable rates of LF and HF seismicity that would indicate the magmatic-hydrothermal system is in a stable open state.

Our results suggest that PRVs can experience several-year-long periods, or cycles, of instability marked by variable seismicity rates, eruptions (i.e. multiple explosions within a period) and isolated explosions, before returning to a phase of elevated but relatively constant rates of seismic or degassing activity. Not only has this pattern of seismicity been observed at Telica during its last major eruption cycle in 1999–2000 (Rodgers et al., 2013), but similar long-term patterns of stable and unstable seismicity rates to those documented here have also been observed at other PRVs: The 1999 eruption of Shishaldin, Alaska was preceded by a short-lived seismic swarm of ~60 events per day; however, much larger seismic swarms of up to ~250 seismic events per day occurred in the following years (Petersen et al., 2006). In 2005 Ngauruhoe, New Zealand, became persistently restless after a 30 year repose interval, and since 2005 has experienced variable seismicity rates between ~5 and ~60 events per day from early 2005 until 2010 that were not associated with any explosive or eruptive activity (Jolly et al., 2012). Finally, Turrialba Volcano, Costa Rica, experienced an increase in seismicity from less than 100 events per day in January 2000, to over 2000 events per day in March 2001, again with no accompanying eruptive activity (Tassi et al., 2004). Therefore it may be appropriate to characterise PRVs as having phases of 'stability' and 'instability' rather than 'quiescence' and 'eruption'. In this paradigm, unstable phases are characterised by strongly fluctuating rates of seismicity, changes in the spectral content of seismic events, and possible explosive activity; whereas stable phases are characterised by steady high-rates of seismicity, consistent spectral content of seismic events, steady degassing, and no explosive activity. We suggest that stable phases represent a well-established system of open-system degassing and that unstable phases represent repeated transitions between open and closed-system degassing at various timescales (from months to hours). This model has implications for eruption forecasting at PRVs where the recognition of the onset of a period of seismic instability indicates that the shallow volcanic system is unable to remain in an open-vent state and that explosions are likely. However, we note that for larger magmatic eruptions the precursory seismic behaviour may be entirely different, which highlights the difficulty of volcano monitoring at persistently restless volcanoes. Ultimately, continued long-term seismic observation and analysis, combined with detailed gas and geodetic observation, is crucial to understand the processes that characterise and drive the transitions between stable and unstable phases at PRVs.

6. Conclusions

We analysed seismicity from a three-year deployment of a broadband seismic network on Telica Volcano, Nicaragua, with the goal of characterising seismicity at a persistently restless volcano during periods of eruptive and non-eruptive activity, and investigating the volcanic processes that drive the transition between these two phases of activity. We demonstrate that both LF and HF seismicity rates at Telica are highly variable and we propose that repeated patterns of high-to-low seismicity rates represent transitions between open-system and closed-system degassing. Furthermore, we suggest that the long-term patterns of seismicity at Telica and other PRVs are characterised by 'stable' or 'unstable' phases, as opposed to 'quiescent' and 'active' phases. In this paradigm stable phases are characterised by steady high event rates and consistent spectral content, and represent a well-established open-system degassing process. Unstable phases are characterised by highly variable rates of seismicity, changing spectral content and explosive activity and represent repeated transition between open and closed-system degassing. Our observations have important implications for eruption forecasting at Telica and other PRVs, where the recognition of unstable phases of seismic activity, including but not limited to sudden or gradual declines in seismic activity, may indicate that the open-system degassing process cannot be sustained and that explosions are likely.

Acknowledgements

We thank the staff at INETER for on-going assistance and support during deployment of this network. In particular we thank INETER technician Allan Morales for his invaluable field assistance. We thank Jim Normandeau (UNAVCO) for assistance in network installation and ongoing instrumentation advice. We also thank Glenn Thompson and Mike West for advice on using Antelope software and we are extremely grateful to Simon Rodgers for development of the software that was used for spectral analysis in this manuscript. Work undertaken at USF was funded by NSF grant EAR-0911366 to D. Roman and EAR-0911546 to P. LaFemina. Work undertaken at Oxford was completed while funded on NERC STREVA grant NE/J020001/1. We would like to thank two anonymous reviewers for constructive reviews of this manuscript.

References

Buurman, H., West, M.E., 2010. Seismic precursors to volcanic explosions during the 2006 eruption of Augustine Volcano. In: Power, J.A., Coombs., M.L., Freymueller, J.T. (Eds.), The 2006 eruption of Augustine Volcano. U.S.G.S Professional Paper 1769, Alaska, pp. 41–57.

Byerlee, J., 1978. Friction of rocks. Pure. Appl. Geophys. 116, 615–626.

Chouet, B.A., Matoza, R.S., 2013. A multi-decadal view of seismic methods for detecting precursors of magma movement and eruption. J. Volcanol. Geotherm. Res. 252, 108–175.

Dixon, J.P., Stihler, S.D., Power, J.A., Tytgat, G., Estes, S., Moran, S.C., Paskievitch, J., McNutt, S.R., 2006. Catalog of earthquake hypocenters at Alaskan volcanoes: January 1 through December 31, 2010.

Endo, E.T., Murray, T., 1991. Real-time seismic amplitude measurement (RSAM): a volcano monitoring and prediction tool. Bull. Volcanol. 53, 533–545.

Geirsson, H., Rodgers, M., LaFemina, P., Witter, M., Roman, D., Muñoz, A., Tenorio, V., Alvarez, J., Jacobo, V.C., Nilsson, D., Galle, B., Feineman, M.D., Furman, T., Morales, A., 2014. Multidisciplinary observations of the 2011 explosive eruption of Telica volcano, Nicaragua: Implications for the dynamics of low-explosivity ash eruptions. J. Volcanol. Geotherm. Res. 271, 55–69.

Jolly, A.D., Neuberg, J., Jousset, P., Sherburn, S., 2012. A new source process for evolving repetitious earthquakes at Ngauruhoe volcano, New Zealand. J. Volcanol. Geotherm. Res. 215–216, 26–39.

Kilburn, C., 2012. Precursory deformation and fracture before brittle rock failure and potential application to volcanic unrest. J. Geophys. Res. 117, B02211.

Lahr, J.C., Chouet, B.A., Stephens, C.D., Power, J.A., Page, R.A., 1994. Earthquake classification, location, and error analysis in a volcanic environment: implications for the magmatic system of the 1989–1990 eruptions at Redoubt Volcano, Alaska. J. Volcanol. Geotherm. Res. 62, 137–151.

Lienert, B.R., Havskov, J., 1995. A computer program for locating earthquakes both locally and globally. Seismol. Res. Lett. 66, 26–36.

McNutt, S.R., 1996. Seismic monitoring and eruption forecasting of volcanoes: a review of state of the art and case histories. In: Scarpa, R., Tilling, R. (Eds.), Monitoring and mitigation of volcano hazards. Springer, pp. 99–147.

McNutt, S.R., 2005. Volcanic seismology. Annu. Rev. Earth Planet. Sci. 33, 461–491.

McNutt, S.R., Jacob, K.H., 1986. Determination of large-scale velocity structure of the crust and upper mantle in the vicinity of Pavlof Volcano, Alaska. J. Geophys. Res. 91, 5013–5022.

Minakami, T., 1974. Seismology of volcanoes in Japan, in: Developments in solid earth geophysics. In: Civetta, L., Gasparini, P., Luongo, G., Rapolla, A. (Eds.), Physical volcanology. 6. Elsevier, Amsterdam, pp. 1–27.

Petersen, T., Caplan-Auerbach, J., McNutt, S.R., 2006. Sustained long-period seismicity at Shishaldin Volcano, Alaska. J. Volcanol. Geotherm. Res. 151, 365–381.

Powell, T.W., 2004. Characterisation of volcano-seismic events and their relation to volcanic processes in the Montserrat eruption. University of Leeds, UK.

Roche, O., van Wyk de Vries, B., Druitt, T.H., 2001. Sub-surface structures and collapse mechanisms of summit pit craters. J. Volcanol. Geotherm. Res. 105, 1–18.

Rodgers, M., Roman, D.C., Geirsson, H., LaFemina, P., Muñoz, A., Guzman, C., Tenorio, V., 2013. Seismicity accompanying the 1999 eruptive episode at Telica Volcano, Nicaragua. J. Volcanol. Geotherm. Res. 265, 39–51.

Roman, D.C., Cashman, K.V., 2006. The origin of volcano-tectonic earthquake swarms. Geology 34, 457–460.

Siebert, L., Simkin, T., 2002. Volcanoes of the World: an Illustrated Catalog of Holocene Volcanoes and their eruptions. Smithsonian Institution, Global Volcanism Program Digital Information Series (GVP-3).

Stix, J., 2007. Stability and instability of quiescently active volcanoes: The case of Masaya, Nicaragua. Geology 35, 535–538.

Tassi, F., Vaselli, O., Barboza, V., Fernandez, E., Duarte, E., 2004. Fluid geochemistry and seismic activity in the period 1998-2002 at Turrialba Volcano (Costa Rica). Ann. Geophys. 47, 1501–1511.
Tenorio, V., 1993. Boletín Mensual, Sismos y Volcanes de Nicaragua.
Thelen, W., West, M., Senyukov, S., 2010. Seismic characterization of the fall 2007 eruptive sequence at Bezymianny Volcano, Russia. J. Volcanol. Geotherm. Res. 194, 201–213.
Voight, B., 1988. A method for prediction of volcanic eruptions. Nature 332, 125–130.
Voight, B., Sparks, R.S.J., Miller, A.D., Stewart, R.C., Hoblitt, R.P., Clarke, A., Ewart, J., Aspinall, W.P., Baptie, B., Calder, E.S., Cole, P., Druitt, T.H., Hartford, C., Herd, R.A., Jackson, P., Lejeune, A.M., Lockhart, A.B., Loughlin, S.C., Luckett, R., Lynch, L., Norton, G.E., Robertson, R., Watson, I.M., Watts, R., Young, S.R., 1999. Magma flow instability and cyclic activity at Soufriere hills volcano, Montserrat, British West Indies. Science 283, 1138–1142 (80-.).